PUBLISHED BY IOP PUBLISHING FOR SISSA MEDIALAB

RECEIVED: *November 17, 2012*
ACCEPTED: *February 13, 2013*
PUBLISHED: *March 18, 2013*

TECHNICAL REPORT

Expansion cone for the 3-inch PMTs of the KM3NeT optical modules

The KM3NeT collaboration

E-mail: o.kavatsyuk@rug.nl

ABSTRACT: Detection of high-energy neutrinos from distant astrophysical sources will open a new window on the Universe. The detection principle exploits the measurement of Cherenkov light emitted by charged particles resulting from neutrino interactions in the matter containing the telescope. A novel multi-PMT digital optical module (DOM) was developed to contain 31 3-inch photomultiplier tubes (PMTs). In order to maximize the detector sensitivity, each PMT will be surrounded by an expansion cone which collects photons that would otherwise miss the photocathode. Results for various angles of incidence with respect to the PMT surface indicate an increase in collection efficiency by 30% on average for angles up to 45° with respect to the perpendicular. Ray-tracing calculations could reproduce the measurements, allowing to estimate an increase in the overall photocathode sensitivity, integrated over all angles of incidence, by 27% (for a single PMT). Prototype DOMs, being built by the KM3NeT consortium, will be equipped with these expansion cones.

KEYWORDS: Optical detector readout concepts; Instrument optimisation; Cherenkov detectors; Large detector systems for particle and astroparticle physics

doi:10.1088/1748-0221/8/03/T03006

Contents

2013 JINST 8 T03006

1 Introduction

KM3NeT [1] is a future deep-sea research infrastructure hosting a neutrino telescope with a volume of several cubic kilometers to be constructed in the Mediterranean Sea. The design, construction and operation of the KM3NeT neutrino telescope will be pursued by a consortium formed by numerous research institutes currently involved in the ANTARES [2], NEMO [3] and NESTOR [4] pilot projects. These Mediterranean pilot projects have been exploring the technologies, building prototypes and deploying small scale telescopes. Since May 30, 2008, the ANTARES underwater neutrino telescope has been fully operational. Although being the largest neutrino detector viewing the Galactic Center through the Earth as a shield against atmospheric muons, an efficient search for high-energy (1–1000 TeV) neutrinos originating from galactic and extra-galactic sources requires a much larger deep-sea Neutrino Telescope.

The detection principle exploits the measurement of Cherenkov light emitted by charged secondary particles resulting from neutrino interactions in the matter surrounding the telescope. Accurate measurements of the light arrival times and amplitudes are required. These, together with a precise knowledge in real time of the positions and orientations of the photosensors, are mandatory to reconstruct the direction of the neutrinos with an angular resolution better than 0.3° for neutrino energies above a few TeV. Such a precision on the measurement of the neutrino direction is a key ingredient to reach the necessary sensitivity on point-like cosmic neutrino sources in a few years of operation. In order to improve the rejection of environmental background and to increase the sensitivity to high energy neutrinos, a digital optical module (DOM) with an arrangement of 31 3-inch photomultiplier tubes (PMTs) has been designed.

2 Multi-PMT DOM

The multi-PMT DOM is an alternative to the conventional approach using one single 10-inch PMT or larger, and has several advantages. The total photocathode area that can be fitted in a standard 17-inch diameter glass pressure sphere is significantly larger when using many small PMTs as compared to a single large PMT. The segmentation of the detection area in the multi-PMT DOM will aid in distinguishing single-photon from multi-photon hits. Two-photon hits can be unambiguously recognized if the two photons hit separate tubes. Photons arriving in a plane wave from a particular direction may be sensed by 7 PMTs on average. The probability that a signal corresponding to two photo-electrons in a single 10-inch PMT is shared by two small PMTs is thus (1 - 1/7) $\approx$ 0.85 [1]. Small PMTs can offer a quantum efficiency above 30%, provide a small transit time spread and do not require shielding from the Earth's magnetic field. Also the reliability of the multi-PMT DOM is higher since a failure of a single PMT will have much less impact on the performance of the total DOM as compared to an optical module housing a single large PMT. Since handling the data flow from the large number of PMTs in such a DOM becomes challenging, a cost-efficient readout system is being developed [1, 5] with complete digitization inside the DOM.

The housing of the multi-PMT DOM (figure 1) is a transparent 17-inch glass sphere (VITROVEX glass [7], wall thickness 14 mm), built to withstand the ambient hydrostatic pressure up to 600 bar. The sphere is separated into two hemispheres and contains the PMTs, the high-voltage power supplies, front-end and readout electronics. The PMTs are suspended in a foam support structure carrying 19 tubes in the lower and 12 in the upper hemisphere.

The center of the front face of each PMT is placed 4 mm from the inner surface of the glass sphere. Optical gel fills the cavity between the foam support or the PMT front face and the glass in order to assure optical contact (optical coupler). The foam support and the gel are sufficiently flexible to allow for the deformation of the glass sphere under the hydrostatic pressure.

A mushroom-shaped aluminum structure transfers the heat generated by the DOM electronics via the glass sphere to the seawater. For accurate muon reconstruction, it is necessary to know the PMT positions with an accuracy of about 10 cm, and for this a position calibration system is required. The multi-PMT DOM contains three calibration devices: the compass-tiltmeter, the acoustic piezo sensor, and the nanobeacon, a compact low-cost nanosecond light flasher. More details on the multi-PMT DOM can be found in ref. [6, 8].

The dense packing constrains the space available for power supply and readout in the center of the DOM. However, the optimal electro-optical design of the PMT leaves extra space between neighboring PMTs on the inner surface of the sphere, surrounding the cathode entrance window (see figure 1). To exploit this extra space for light collection, a reflector (expansion cone) will be employed to guide additional light to the photocathode. The Photonis XP53B20 PMT, that passed the specification requirements of KM3NeT except the dark-currect performance, has a concave-convex shaped glass window with a thickness of about 9 mm at the circumference and provides a curved photocathode for optimum light collection and fast timing properties. PMTs with similar performance parameters are presently commercially available from several manufactures. The thickness of the entrance window leaves space available for the entrance of light from the side onto the curved photocathode. Results of tests will be presented for an expansion cone made of silicone gel [9] which is shaped and kept in place by an aluminum structure serving as reflector,

2013 JINST 8 T03006

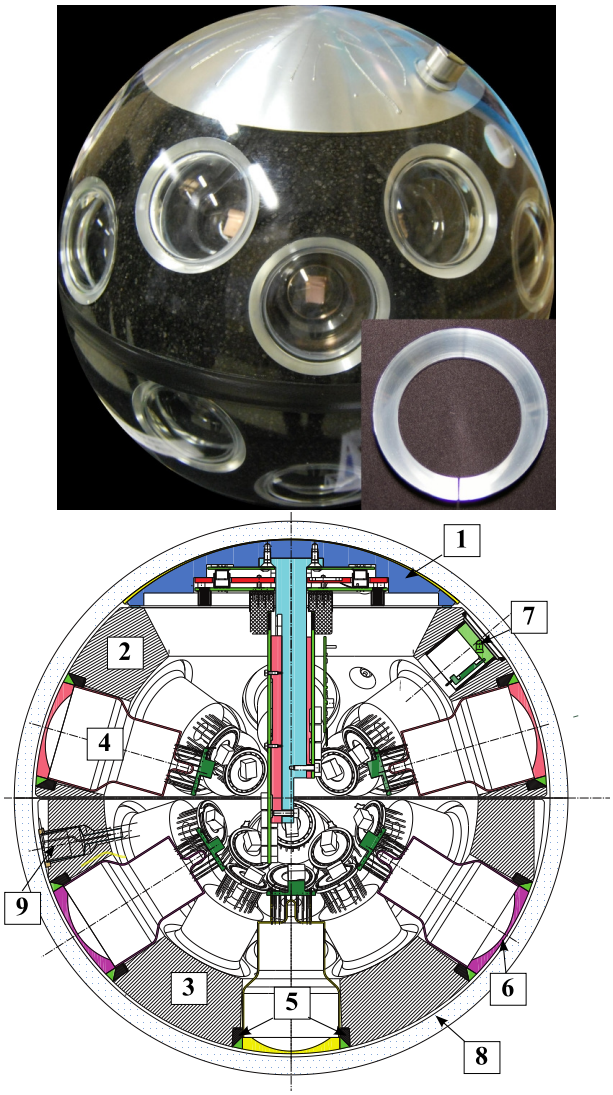

Figure 1. *Upper panel*: a mechanical reference model of a multi-PMT DOM with reflectors surrounding 3-inch PMTs. A single reflector is shown in the insert. *Lower panel*: cross section of a multi-PMT DOM [6] revealing the dense packing of readout electronics inside. Numbers refer to: 1-Heat conductor, 2,3-Foam cores, 4-PMT with PMT base, 5-Expansion cone, 6-Optical coupler, 7-Nanobeacon, 8-Glass sphere, 9-Piezo element.

shown schematically in figure 2. The reflectivity of the 45° tilted surface was improved by silver evaporation. In order to demonstrate the potential benefit of the expansion cone, measurements in air and with a single PMT have been performed.

3 The expansion cone: idea and implementation

Each PMT in the multi-PMT DOM will be surrounded by an expansion cone designed to collect photons that would otherwise miss the photocathode, thus increasing the effective photocathode area (figure 1). The main idea behind such an expansion cone is demonstrated in figure 3. The

2013 JINST 8 T03006

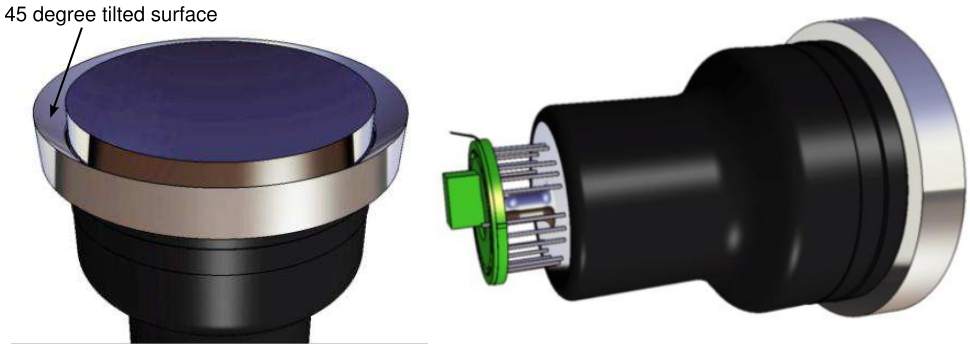

Figure 2. A drawing of the expansion cone mounted on a PMT.

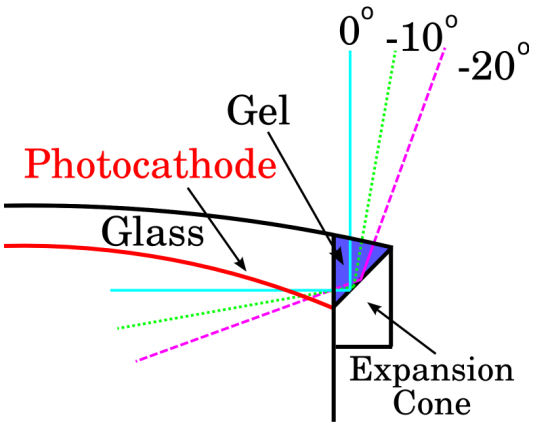

Figure 3. The idea of light collection by an expansion cone.

light that comes aside of the PMT entrance window is reflected by the 45° tilted surface into the photocathode. Ray-tracing simulations were performed for various opening angles of the expansion cone. The opening angle of 45° is optimized for maximum collection of light coming perpendicular to the PMT entrance window, which is essential for the direction reconstruction. The silicone gel serves as an optical interface, having a refractive index of 1.40 and the refractive index of the PMT entrance window is 1.54 (for photons of 420 nm wavelength).

For the performance tests, a 3-inch diameter Photonis XP53B20 PMT was used with main characteristics listed in table 1. The Photonis XP53B20 tube has a compact Box & Linear structured 10-stage electron multiplier allowing a short tube design required for a compact multi-PMT DOM. Moreover, it has a convex-shaped entrance window matched to the curvature of the glass sphere of the optical module (figure 1). In order to test the idea of such an expansion cone, measurements with a simplified setup were done. In comparison to the expansion cone to be used in the multi-PMT DOM [6], a cone with a larger diameter of 104 mm instead of 92 mm was manufactured from aluminum (figure 4). This cone allows to fill silicon gel up to the level of 1 mm above the edge at the circumference of the PMT, as shown in figure 5, without using a glass sphere. Further, the larger cone allows to eliminate edge effects as they appear in the test setup due to the finite size of the test beam.

2013 JINST 8 T03006

Table 1. Characteristics of the used XP53B20 Photonis PMT from specifications and measurements.

	Photonis XP53B20
Window material	lime glass
Window curvature, R[mm]	198
Photocathode	improved Bi-alkali
QE [%]	33 (404 nm) [10]
Spectral range [nm]	290–700
Multiplier structure	10 stage Box & Linear
Time resolution, σ [ns]	2.30(0.02)*
Transit Time Spread [ns]	0.4*
Dark count rate [kHz]	5*

*Detailed results and method described in [11].

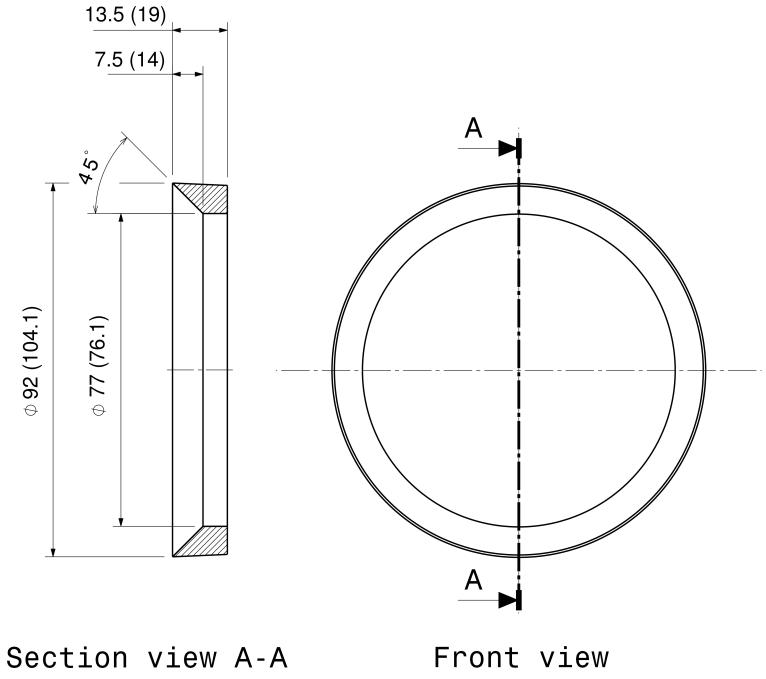

Figure 4. The expansion cone geometry to be used in the multi-PMT DOM. For the performance tests an expansion cone with sizes as given in brackets was manufactured (details in text).

4 Test bench

The performance of the expansion cone was measured using a PMT socket with a built-in pre-amplifier (pre-amplification factor 62) in order to reduce heat dissipation, electronic noise and dark current. It allowed the operation at a PMT gain 1.2×10^6 with a high voltage of 950 V.

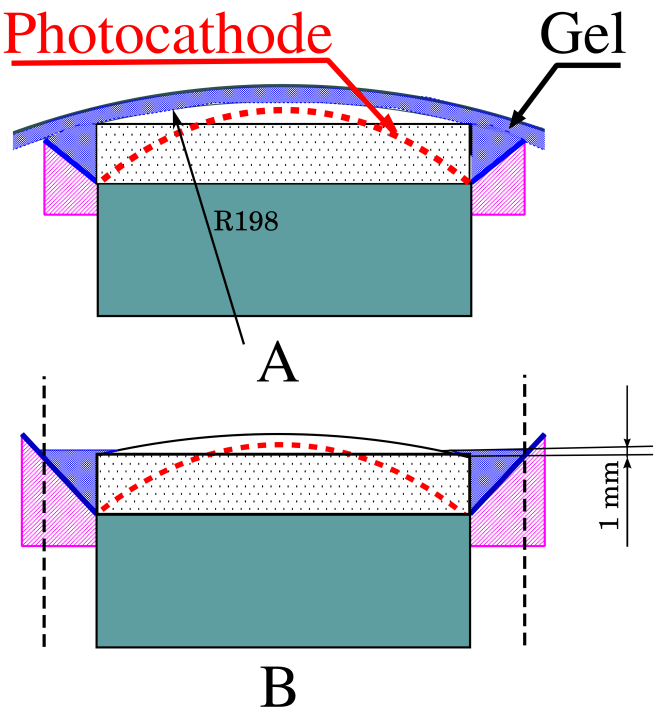

Figure 5. Silicon gel filled in the: *A*. Expansion cone geometry used in the multi-PMT DOM; *B*. Geometry used for tests. Silicone gel filled 1 mm above the edge at the circumference of the PMT. For the analysis, only data points limited to a radius X<46 mm (dotted lines) were considered.

A PMT with the mounted expansion cone was placed inside a light-tight box (DarkBox). As a pulsed light source a laser[1] with wavelength $\lambda = 405$ nm and time jitter of < 70 ps between trigger and pulse was used. Additionally, a variable neutral density filter allowed to reduce intensities down to the level of single photo-electrons per pulse. A trigger output from the laser controller was used as a start signal for the data acquisition. The light from the laser was guided with a light fiber (core diameter 0.6 mm) inside the DarkBox and shone perpendicularly to the entrance window. This setup allowed a spot size of FWHM=1.4 mm at the center of the entrance window with a distance of 3 mm from the fiber to the PMT. Signal shapes were recorded by a fast sampling ADC.[2] A remote-controlled 2D scanning system placed inside the DarkBox allowed precise measurements of the photocathode homogeneity and sensitivity with respect to position and angle of incidence. The scanning system consisted of two linear stages that allowed scanning in horizontal and vertical directions, equipped with stepper motors providing a repeatability of 1.5 μm. The orientation of a PMT in the setup was defined by the orientation of the dynode structure. The origin of the coordinate system was the center of the entrance window. The Y axis lies in the plane of symmetry of the electron multiplier chain, perpendicularly to the dynodes. In practice, the correspondence between pin layout and inner configuration was used: the Y axis points from the anode to the first dynode pin (figure 6).

[1] Hamamatsu PLP10-40 laser diode head (wavelength 405 nm) with C10196 Controller.
[2] Acqiris DC282 digitizer with 10 bit resolution and 8 GS/s sampling rate.

2013 JINST 8 T03006

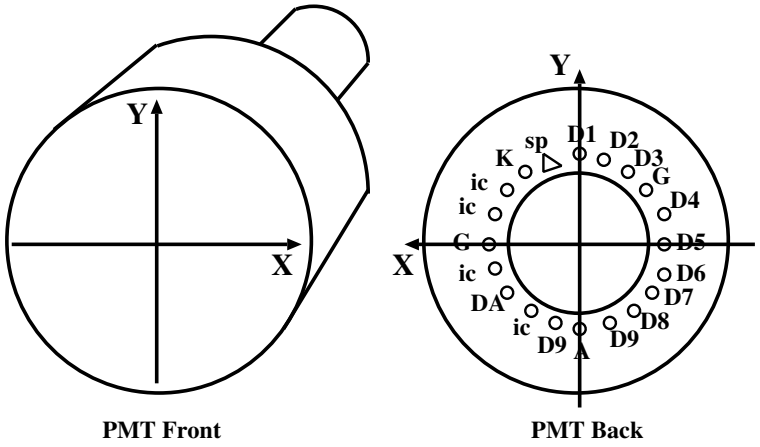

Figure 6. Coordinate system with origin at the center of the PMT entrance window used for the photocathode scan. The correspondence between the inner configuration of the electron multiplier and the pin-layout was used.

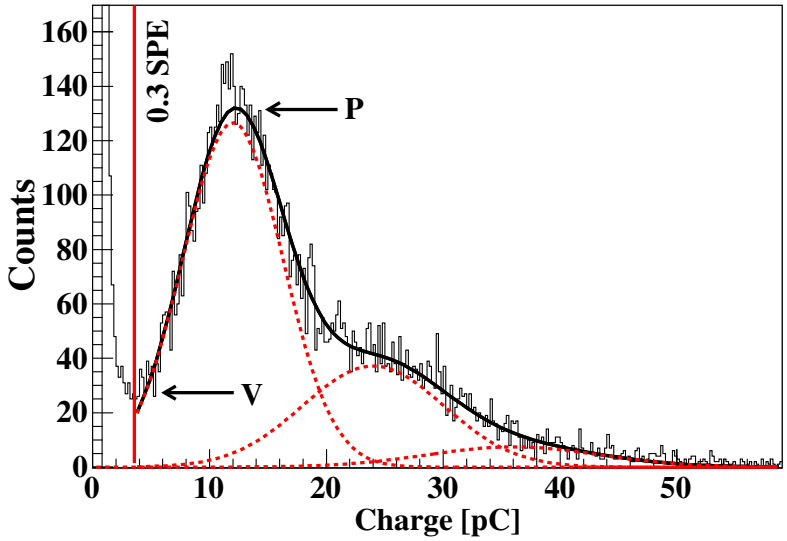

Figure 7. Typical measured charge distribution. PMT gain 1.2×10^6, pre-amplification 62. The position of the peak (P) and valley (V) are indicated.

5 Results

A typical measured charge spectrum for a single point on the photocathode (center) is shown in figure 7. The position of the single-photoelectron (SPE) peak was determined and the PMT gain was derived. In figure 7 the contributions of one-, two- and three-PEs are separated by applying a deconvolution procedure according to [12]. The operation of a tube at a gain of 1.2×10^6 provides a good peak-to-valley ratio of about five. In order to determine the relative collection efficiency, the fraction of events with a charge above 0.3 SPE out of a total number of 20,000 accepted triggers was obtained for various points on the photocathode. The number of selected events for the center of the PMT was about 10,000.

2013 JINST 8 T03006

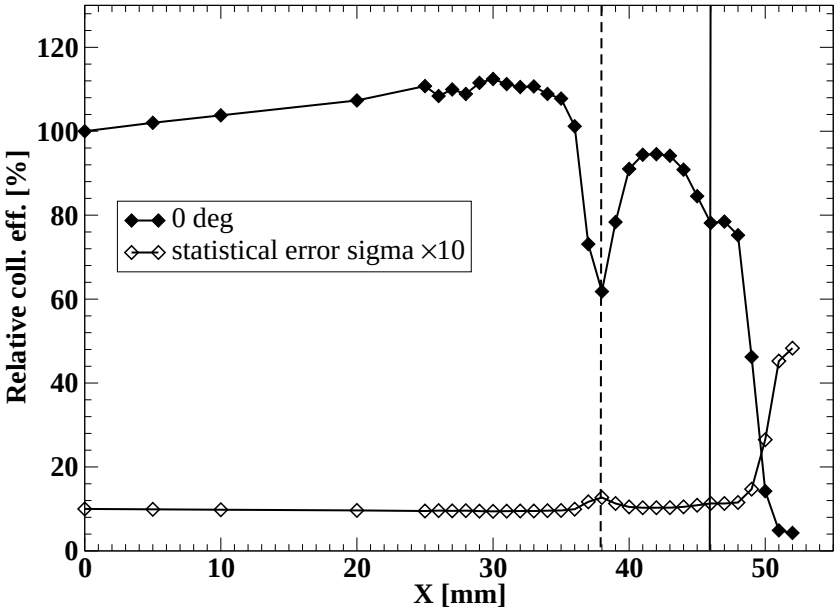

Figure 8. The relative collection efficiency for photon incidence perpendicular to the photocathode surface as a function of the radial position X on the photocathode, normalized to 100% at the center (X=0). Vertical lines indicate the position of the contact between the PMT and the expansion cone (dashed line), and the size of the expansion cone used in the multi-PMT DOM (solid line), respectively.

In this work we compare the number of measured photon pulses for various positions on the photocathode and for a number of angles of incidence. The number of counts N_d is defined as $N_d = PDE \cdot N_p = QE \cdot CE \cdot N_p$, where PDE is the photon detection efficiency, N_p the number of incident photons, QE the quantum efficiency and CE the collection efficiency. We use the ratio $N_d(X)/N_d(0)$, where $N_d(0)$ is the number of counts collected in the centre of the photocathode, and $N_d(X)$ at any other point X. In the ratio, QE and N_p drop out (since we measure under the same conditions), resulting in the ratio of collection efficiencies $CE(X)/CE(0)$ or the relative collection efficiency. We assumed the collection efficiency in the centre of the entrance window (photocathode) to be 100% (for perpendicular incidence) and investigated the difference for the other points distributed on the photocathode and for various angles of incidence.

The relative collection efficiency as a function of the position on the photocathode is shown in figure 8 for the perpendicular incidence (0°). This results were obtained for a scan across the photocathode along the X-axis, measured at a temperature of 21°C. A dip in the relative collection efficiency curve observed at about X = 38 mm can be explained by the expected decrease in the reflection on the contact between the PMT and the expansion cone and the thickness of the glass wall. However, an additional experiment with a cone that could be moved axially has shown, that the observed decrease is not only caused by the effects mentioned above but also by the shift along the axial direction of the expansion cone relative to the photocathode. This assumption was confirmed by the performed ray-tracing simulations (see section 6) and in previous extensive tests with an expansion cone made of PMMA [13]. The shoulder at 46–48 mm corresponds to the level to which the gel is filled (see figure 5).

2013 JINST 8 T03006

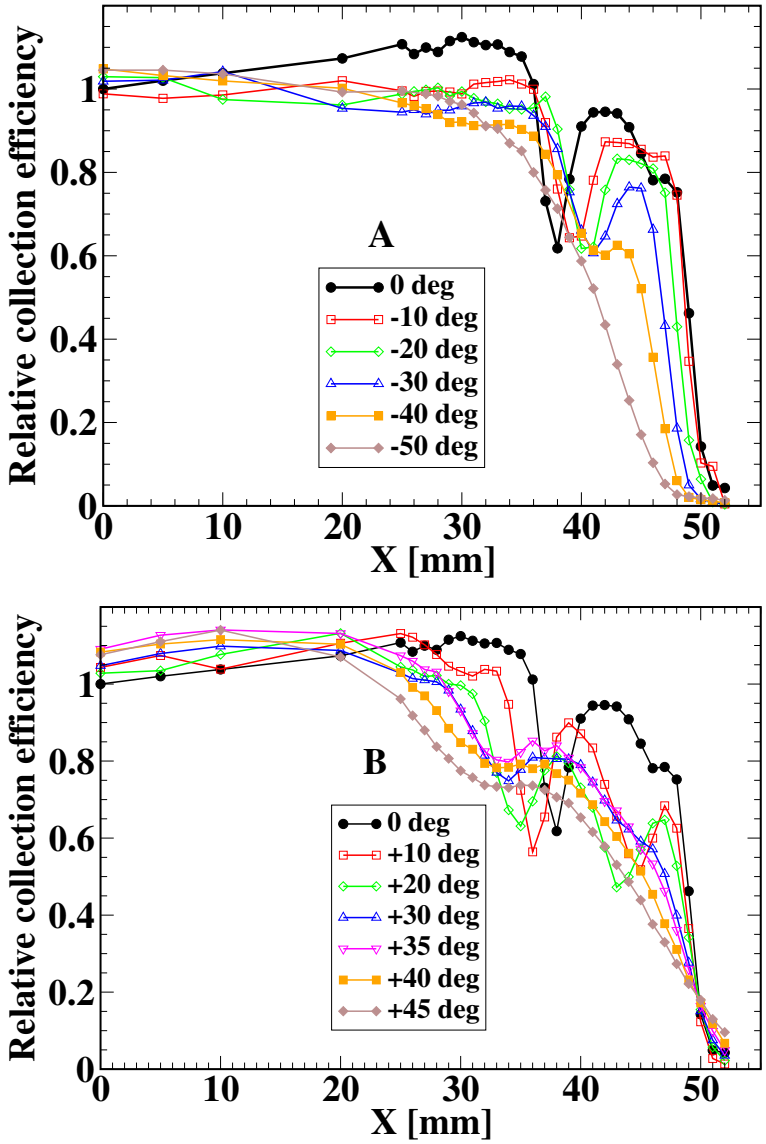

Figure 9. Measured relative collection efficiency as a function of the radial position X for various angles of incidence (see figure 3); *Upper panel:* for negative angles of incidence; *Lower panel:* for positive angles of incidence.

Since every measured point X_v in the scan along the X direction represents an annulus with a width equal to the distance ΔX_v of neighboring measured points, weights $W(X_v)$ are applied in order to account for the respective annular areas: $W(X_v) = \int_{\Delta X_v} 2\pi X dX$. The larger spacing between data points in the region 10 mm $<$ X $<$ 25 mm resulted in larger weighting factors for these points.

Results for the measurements with various angles of incidence are presented in figure 9. The definition of the sign of the angles of incidence is introduced in figure 3. In order to estimate the benefit of the expansion cone, the gained collection efficiency was calculated. For each angle of incidence the integral C_{PMT} was taken under the collection efficiency curve (figure 9) for the

2013 JINST 8 T03006

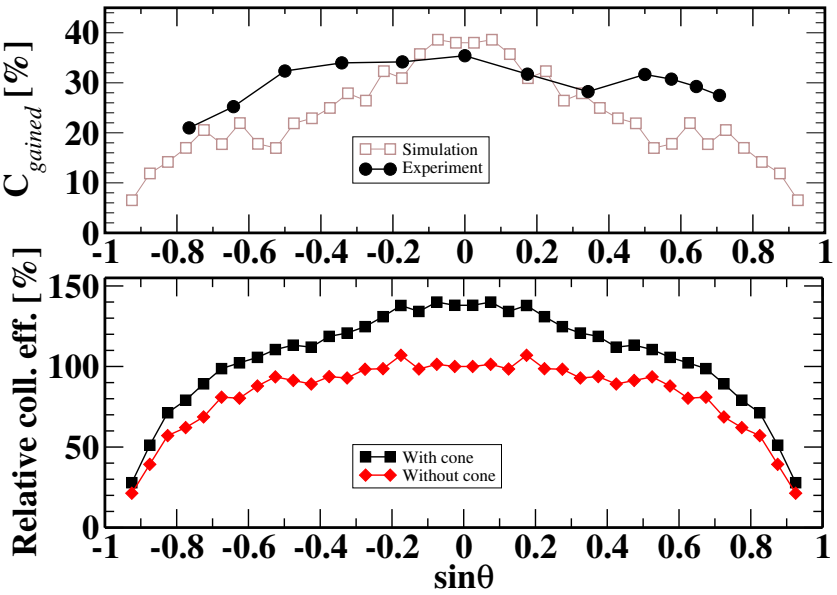

Figure 10. *Upper panel*: gained collection efficiency along the X-axis according to eq. 5.1, as a function of sin of the angle of incidence θ. All presented data points have error bars of $C_{\text{gained}}[\%] \pm 0.04[\%]$. Results of the performed ray-tracing simulations are shown for comparison. *Lower panel*: results of the ray-tracing simulations. Collection efficiency as a function of the angle of incidence for a single PMT with and without expansion cone (squares and diamonds, respectively).

range (0 mm, 38 mm), corresponding to the light entering directly in the photocathode. The integral $C_{PMT+Cone}$ was taken for the range (0 mm, 46 mm) corresponding to the radial range of the expansion cone to be used in KM3NeT (figure 5). In section 6 we demonstrate that the procedure of truncating a larger cone provides a realistic estimate of the light collection for the combination of PMT and expansion cone (*PMT + Cone*). Finally, the gained collection efficiency C_{gained} was estimated as a ratio

$$C_{\text{gained}} = \frac{C_{PMT+Cone} - C_{PMT}}{C_{PMT}} \times 100\%, \tag{5.1}$$

where $C_{PMT+Cone}$ and C_{PMT} are the collection efficiencies of the combination *PMT + Cone* and PMT, respectively.

Results for the measurements under various angles of incidence are presented in figure 10, revealing an increase in collection efficiency by 30% on average for angles of incidence from -50° to $+45^\circ$, with a maximum of 35% for perpendicular incidence.

The results presented above were performed with angles of incidence varied in a plane parallel to the X-axis (*A* in figure 11), because of limitations of the scanning system. In order to account for effects for angles in the plane parallel to the Y-axis, measurements with configuration *B* (figure 11) were performed. Points with radius 41, 42, 43 and 44 mm were chosen to represent the performance of the expansion cone. Results presented in figure 12 follow a Gaussian-like distribution and agree well with distributions measured in the plane parallel to the X-axis (see figure 10 for comparison, configuration *A* in figure 11). The combined results allow to estimate the expansion cone performance rather well from data obtained for angles of incidence varied in one plane.

2013 JINST 8 T03006

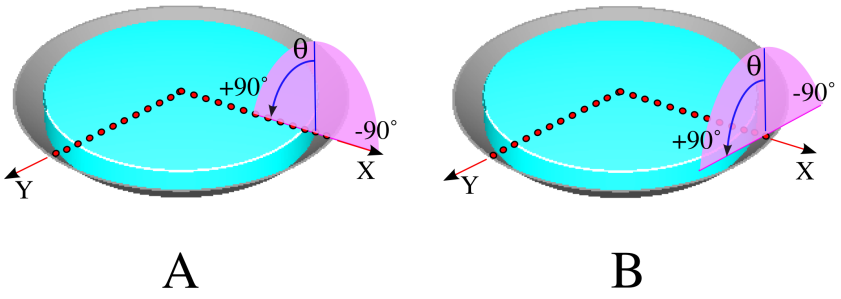

Figure 11. The expansion cone performance was tested with angles of incidence varied in two planes: parallel to the X-axis (*A*) and to the Y-axis (*B*).

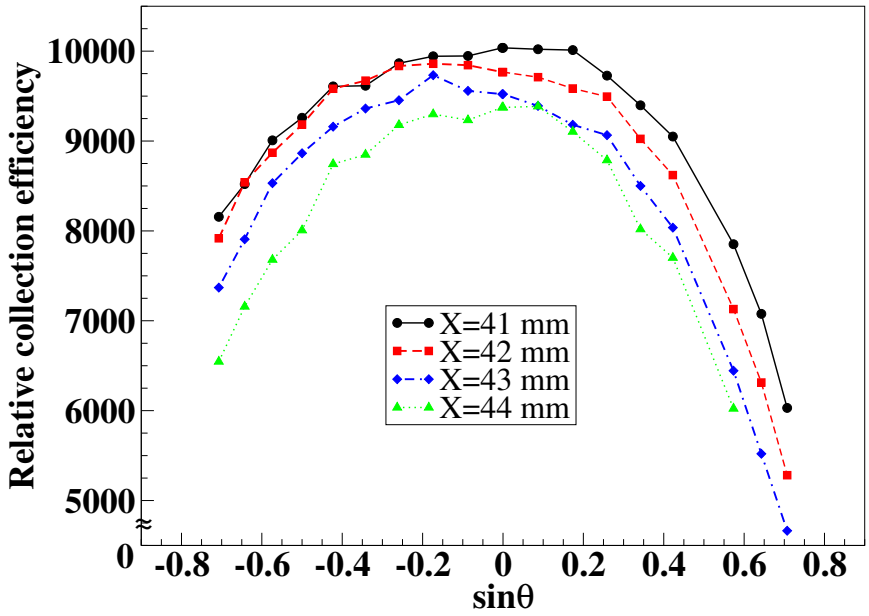

Figure 12. Measured relative light collection efficiency as a function of sin of the angle of incidence θ in the plane parallel to the Y-axis (*B* in figure 11), for various radial positions on the expansion cone.

6 Simulation

Ray-tracing calculations were performed by using SLitrani [14], a general purpose Monte-Carlo program simulating light propagation. Even with a very simplified geometry (photocathode and aluminum expansion cone), shown in figure 13, the simulations reproduce the essential features of the distribution for the measured collection efficiency at perpendicular incidence (see figure 14 and 8 for comparison). For this purpose a horizontal scan across the photocathode was simulated with light emitted perpendicularly from a light fiber producing a spot size of 1.4 mm FWHM on the photocathode. Results are shown in figure 14. In order to reproduce the experimental data points, a 1 mm axial shift of the expansion cone relative to the photocathode position was introduced. The obtained results, presented in figure 14, with different amplitudes in the contact region, confirm, as discussed in figure 8, the shift in the axial position of the expansion cone. This underlines the importance to know the exact geometry of the photocathode.

2013 JINST 8 T03006

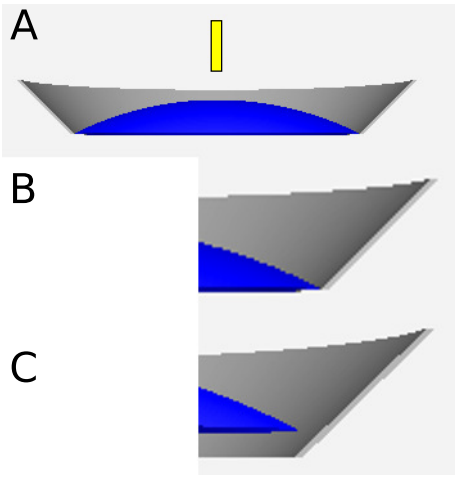

Figure 13. A. Simulated geometry (not to scale). The expansion cone is shown in gray, the photocathode in blue and the light guiding fiber in yellow on part A (used to reproduce the measured results). B. Zoomed view of the contact region between photocathode and expansion cone. C. Zoomed view of the geometry with an expansion cone that is slightly shifted axially relative to the photocathode (situation for the presented data).

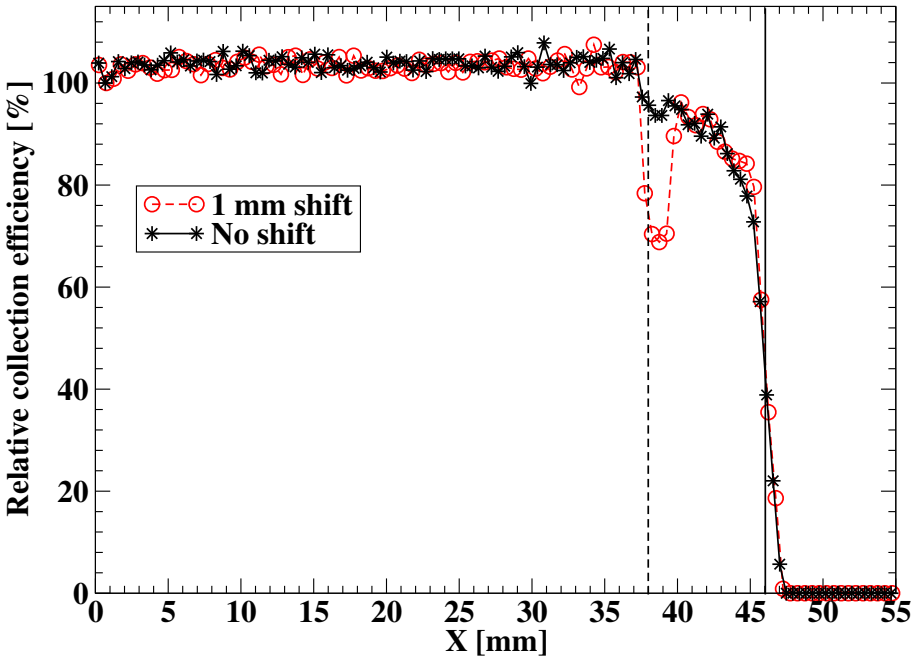

Figure 14. The relative collection efficiency obtained in the ray-tracing calculations with a pencil light beam. *Stars* correspond to the ideally aligned expansion cone of 46 mm radius. *Circles* show results obtained with an expansion cone of 46 mm radius that is shifted axially by 1 mm, reproducing well the essential features of the measured distribution presented in figure 8. Vertical lines indicate the position of the contact between the PMT and the expansion cone (dashed line), and the physical size of the expansion cone used in the multi-PMT DOM at 46 mm (solid line).

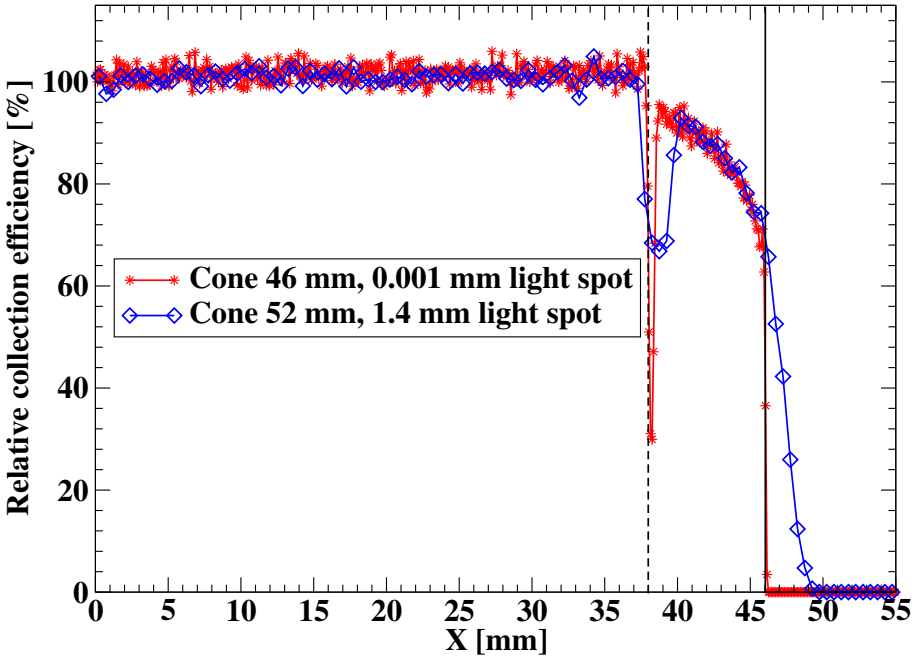

Figure 15. The relative collection efficiency obtained in the ray-tracing calculations with a pencil light beam. *Stars* show results obtained with an expansion cone of 46 mm radius and an almost 0-size light beam. *Diamonds* demonstrate results for an expansion cone of 52 mm radius as used in the measurements shown in figures 8 and 9. Vertical lines indicate the position of the contact between the PMT and the expansion cone (dashed line), and the physical size of the expansion cone used in the multi-PMT DOM at 46 mm radius (solid line).

In section 5 the performance of the expansion cone in the multi-PMT DOM of KM3NeT was estimated by truncating experimental data measured for a 104 mm diameter cone. It should be noted that measurements were done with a light beam of 1.4 mm FWHM. The finite beam size creates edge effects because part of the beam will not be reflected when approaching the edge of the cone. This is demonstrated in figure 15 by comparing simulations for cone diameters of 104 mm and 92 mm performed with light-beam diameters of 1.4 mm and 0.001 mm, respectively. The situation of the almost 0-size light beam corresponds to the situation of single photons hitting the cone in KM3NeT. This situation is very well reproduced by truncating data taken with a finite-size light beam and the larger cone at the radius of the cone which will be implemented in KM3NeT.

In order to estimate the collection efficiency integrated over all angles of incidence, a light emitting disk with 50 cm radius, much larger than the one of a PMT (3.8 cm) was simulated at a distance of 5 cm from the photocathode. In total 2×10^6 photons were emitted. The emission points were distributed uniformly over the light disk surface and the photon directions were uniformly distributed over the solid angle 2π. To compare to a configuration without an expansion cone, a photocathode was simulated together with a light absorbing foam core, to account for shadowing effects (see section 2 and figure 1). These two simulated configurations are illustrated in figure 16. To assure that no light is reflected back to the cone or the photocathode, a totally absorbing plane was included in the simulation. The simulation results reveal an increase in the overall sensitivity, integrated over all angles of incidence, by 27%.

2013 JINST 8 T03006

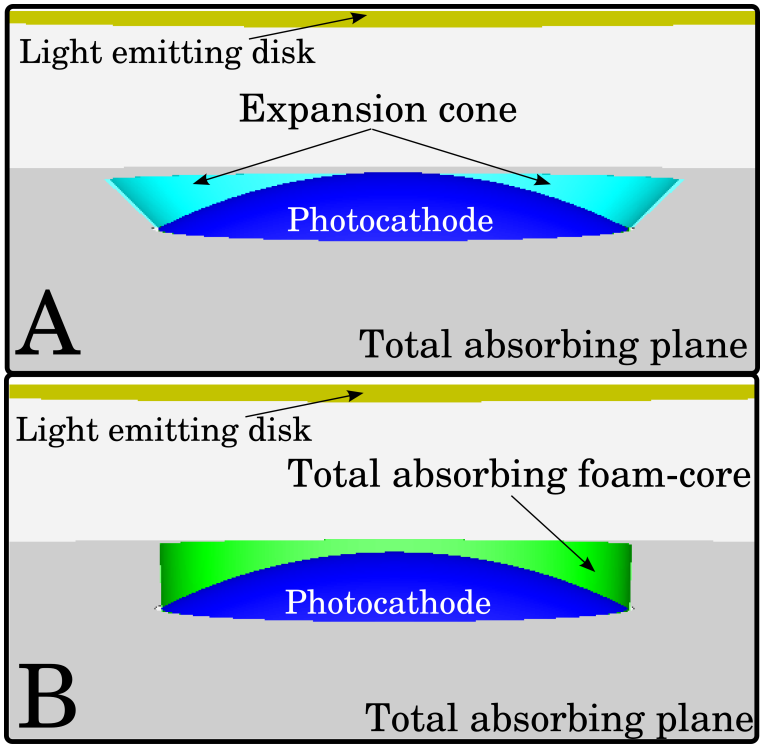

Figure 16. Simulated geometry with (A) and without (B) the expansion cone. The expansion cone, the photocathode, the light emitting disk, the totally absorbing plane, and the foam core are shown.

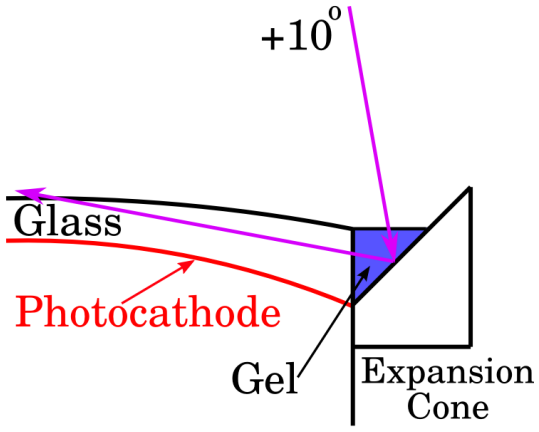

Figure 17. Schematic illustration of a light ray at an angle of incidence of +10°, that can miss the photocathode due to reflection.

The collection efficiency as a function of the angle of incidence was simulated. Results are presented in figure 10. The experimentally obtained curve for the gained collection efficiency (upper panel, figure 10) is slightly asymmetric in comparison to the simulated one. The lower collection efficiency for +10° and +20° results from the curves shown in figure 9B, that exhibit a second dip at X = 45 mm and X = 43 mm, respectively. The cause for this phenomenon is schematically shown in figure 17, where light at certain angles can be reflected above the photocathode.

2013 JINST 8 T03006

7 Summary and discussion

In this work we demonstrated the performance of an expansion cone that is meant to enlarge the sensitive photocathode area of PMTs in a multi-PMT DOM for the future KM3NeT neutrino telescope. The expansion cone consisted of an aluminum ring filled with silicon gel and collects photons that would otherwise miss the photocathode. We have used a simplified experimental geometry to demonstrate the potential benefit of using such an expansion cone, and performed extensive measurements on 3-inch PMTs with concave-convex shaped entrance window. This type of PMT is available for mass production and application in KM3NeT. Note, that the tested expansion cone was larger (exact sizes given in figure 4) in comparison to the one that will be used in the multi-PMT DOM. However, due to the applied pencil light-beam scanning, it was possible to estimate the realistic performance without edge effects for the expansion cone to be used in the multi-PMT DOM by considering only data points limited to a radius $X < 46$ mm (figure 5).

Results for various angles of incidence indicate an increase in collection efficiency by 30% on average for angles of incidence from -50° to +45°, with a maximum of 35% for perpendicular incidence. Ray-tracing simulations estimate an increase of the collection efficiency by 27% integrated over all angles of incidence. Simulations and experiments have shown that the edges of the photocathode are located higher than expected because of lacking information on the photocathode geometry. This effect decreases the cone performance. In the future, precise information on the photocathode geometry will be required from the producer. The proper alignment of the expansion cone relative to the axial position of the photocathode is important to minimize the dip in the collection efficiency at the contact between the expansion cone and the surface of the PMT.

A pencil light-beam has been applied in order to be able to scan precisely the collection efficiency at various locations on the surface of the photocathode. Alternatively, a light beam illuminating the whole PMT equipped with an expansion cone would be advantageous to estimate the cone performance integrated over all angles of incidence. First tests with such a set-up were reported in [15].

In order to obtain the final performance figures of the expansion cone in KM3NeT, measurements under realistic conditions in sea water and with PMTs mounted in a glass sphere will soon be possible using a DOM deployed in ANTARES.

Acknowledgments

This work is supported through the EU, FP6 Contract no. 011937, FP7 grant agreement no. 212252, and the Dutch Ministry of Education, Culture and Science.

References

[1] P. Bagley et al., *KM3NeT Technical Design Report for a Deep-Sea Research Infrastructure in the Mediterranean Sea Incorporating a Very Large Volume Neutrino Telescope*, Technical Report [ISBN:978-90-6488-033-9], http://www.km3net.org/TDR/TDRKM3NeT.pdf.

[2] M. Ageron et al., *ANTARES: The first undersea neutrino telescope*, *Nucl. Instrum. Meth.* **A 656** (2011) 11 [arXiv:1104.1607v2].

2013 JINST 8 T03006

[3] A. Capone et al., *Recent results and perspectives of the NEMO project*, *Nucl. Instrum. Meth.* **A 602** (2009) 47.

[4] P.A. Rapidis, *The NESTOR underwater neutrino telescope project*, *Nucl. Instrum. Meth.* **A 602** (2009) 54.

[5] P. Kooijman, *Multi-PMT optical module*, *Nucl. Instrum. Meth.* **A 567** (2006) 508.

[6] Technical description of the PPM of the KM3NeT detection unit http://www.km3net.org/PPM/KM3NeT_FL_REP_PPM-description.pdf.

[7] http://www.nautilus-gmbh.de/files/vitrovex_instrumentation_housings.pdf.

[8] O. Kavatsyuk, Q. Dorosti-Hasankiadeh and H. Löhner, *Multi-PMT optical module for the KM3NeT neutrino telescope*, *Nucl. Instrum. Meth.* **A 695** (2012) 338.

[9] Wacker SilGel 612, http://www.wacker.com.

[10] B. Herold and O. Kalekin (2009), *Characterisation of PMTs for KM3NeT*, contribution to *ICRC 2009*, Łódź Poland (2009), http://icrc2009.uni.lodz.pl/proc/pdf/icrc0596.pdf.

[11] O. Kavatsyuk, Q. Dorosti-Hasankiadeh and H. Löhner, *Photo-sensors for a Multi-PMT optical module in KM3NeT*, *Nucl. Instrum. Meth.* **A 626-627** (2011) S154.

[12] E.H. Bellamy et al., *Absolute calibration and monitoring of a spectrometric channel using a photomultiplier*, *Nucl. Instrum. Meth.* **A 339** (1994) 468.

[13] O. Kavatsyuk, Q. Dorosti-Hasankiadeh, G. Inguglia and H. Löhner, *Photo-Sensor Characteristics for a Multi-PMT Optical Module in KM3NeT*, contribution to *ICRC 2009*, Łódź Poland (2009), http://icrc2009.uni.lodz.pl/proc/pdf/icrc0767.pdf.

[14] F.X. Gentit, *Litrani: a general purpose Monte-Carlo program simulating light propagation in isotropic or anisotropic media*, *Nucl. Instrum. Meth.* **A 486** (2002) 35.

[15] O. Kalekin, J.J.M. Steijger and H.P. Peek, *Photomultipliers for the KM3NeT optical modules*, *Nucl. Instrum. Meth.* **A 695** (2012) 313.

2013 JINST 8 T03006

The KM3NeT collaboration

S. Adrián-Martínez,[as] M. Ageron,[i] J.A. Aguilar,[p] F. Aharonian,[k] S. Aiello,[u] A. Albert,[m] M. Alexandri,[n] F. Ameli,[ac] E.G. Anassontzis,[d] M. Anghinolfi,[w] G. Anton,[l] S. Anvar,[f] M. Ardid,[as] A. Assis Jesus,[am] J.-J. Aubert,[i] R. Bakker,[an] A.E. Ball,[ao] G. Barbarino,[aa] E. Barbarito,[r] F. Barbato,[aa] B. Baret,[c] M. de Bel,[b] A. Belias,[ao,n] N. Bellou,[ah] E. Berbee,[am] A. Berkien,[am] A. Bersani,[w] V. Bertin,[i] S. Beurthey,[i] S. Biagi,[s] C. Bigongiari,[p] B. Bigourdan,[q] M. Billault,[i] R. de Boer,[am] H. Boer Rookhuizen,[am] M. Bonori,[ad] M. Borghini,[h] M. Bou-Cabo,[as] B. Bouhadef,[ab] G. Bourlis,[o] M. Bouwhuis,[am] S. Bradbury,[aj] A. Brown,[i] F. Bruni,[aq] J. Brunner,[i] M. Brunoldi,[w] J. Busto,[i] G. Cacopardo,[x] L. Caillat,[i] D. Calvo Díaz-Aldagalán,[p] A. Calzas,[i] M. Canals,[e] A. Capone,[ad] J. Carr,[i] E. Castorina,[ab] S. Cecchini,[s] A. Ceres,[r] R. Cereseto,[w] Th. Chaleil,[f] F. Chateau,[f] T. Chiarusi,[s] D. Choqueuse,[q] P.E. Christopoulou,[o] G. Chronis,[n] O. Ciaffoni,[y] M. Circella,[r] R. Cocimano,[x] F. Cohen,[m] F. Colijn,[ah] R. Coniglione,[x] M. Cordelli,[y] A. Cosquer,[i] M. Costa,[x] P. Coyle,[i] J. Craig,[a] A. Creusot,[c] C. Curtil,[i] A. D'Amico,[x] G. Damy,[q] R. De Asmundis,[z] G. De Bonis,[ad] G. Decock,[f] P. Decowski,[am] E. Delagnes,[f] G. De Rosa,[aa] C. Distefano,[x] C. Donzaud,[c,1] D. Dornic,[i] Q. Dorosti-Hasankiadeh,[ai] J. Drogou,[q] D. Drouhin,[m] F. Druillole,[f] L. Drury,[k] D. Durand,[f] G.A. Durand,[f] T. Eberl,[l] U. Emanuele,[p] A. Enzenhöfer,[l] J.-P. Ernenwein,[i] S. Escoffier,[i] V. Espinosa,[as] G. Etiope,[ae] P. Favali,[ae] D. Felea,[ag] M. Ferri,[as] S. Ferry,[f] V. Flaminio,[ab] F. Folger,[l] A. Fotiou,[ao] U. Fritsch,[l] D. Gajanana,[am] R. Garaguso,[ab] G.P. Gasparini,[h] F. Gasparoni,[aq] V. Gautard,[f] F. Gensolen,[i] K. Geyer,[l] G. Giacomelli,[s] I. Gialas,[o] V. Giordano,[x] J. Giraud,[f] N. Gizani,[o] A. Gleixner,[l] C. Gojak,[i] J.P. Gómez-González,[p] K. Graf,[l] D. Grasso,[ab] A. Grimaldi,[u] R. Groenewegen,[an] Z. Guédé,[q] G. Guillard,[af] F. Guilloux,[f] R. Habel,[y] G. Hallewell,[i] H. van Haren,[an] J. van Heerwaarden,[an] A. Heijboer,[am] E. Heine,[am] J.J. Hernández-Rey,[p] B. Herold,[l] M. van de Hoek,[am] J. Hogenbirk,[am] J. Hößl,[l] C.C. Hsu,[am] M. Imbesi,[x] A. Jamieson,[a] P. Jansweijer,[am] M. de Jong,[am] F. Jouvenot,[ak] M. Kadler,[l,2] N. Kalantar-Nayestanaki,[ai] O. Kalekin,[l] A. Kappes,[l,3] M. Karolak,[f] U.F. Katz,[l] O. Kavatsyuk,[ai] P. Keller,[i] Y. Kiskiras,[ao] R. Klein,[l] H. Kok,[am] H. Kontoyiannis,[n] P. Kooijman,[b,am,ar] J. Koopstra,[b,am] C. Kopper,[am,4] A. Korporaal,[am] P. Koske,[ah] A. Kouchner,[c] S. Koutsoukos,[d] I. Kreykenbohm,[l] V. Kulikovskiy,[w,5] M. Laan,[an] C. La Fratta,[ae] P. Lagier,[i] R. Lahmann,[l] P. Lamare,[i] G. Larosa,[as] D. Lattuada,[x] A. Leisos,[o] D. Lenis,[o] E. Leonora,[u] H. Le Provost,[f] G. Lim,[b] C.D. Llorens,[as] J. Lloret,[as] H. Löhner,[ai] D. Lo Presti,[v] P. Lotrus,[f] F. Louis,[f] F. Lucarelli,[ad] V. Lykousis,[n] D. Malyshev,[k,6] S. Mangano,[p] E.C. Marcoulaki,[al] A. Margiotta,[s] G. Marinaro,[ae] A. Marinelli,[ab] O. Mariş,[ag] E. Markopoulos,[ao] C. Markou,[al] J.A. Martínez-Mora,[as] A. Martini,[y] J. Marvaldi,[q] R. Masullo,[ad] G. Maurin,[f,7] P. Migliozzi,[z] E. Migneco,[x] S. Minutoli,[w] A. Miraglia,[x] C.M. Mollo,[z] M. Mongelli,[r] E. Monmarthe,[f] M. Morganti,[ab] S. Mos,[am] H. Motz,[l,8] Y. Moudden,[f] G. Mul,[am] P. Musico,[w] M. Musumeci,[x] Ch. Naumann,[f,9] M. Neff,[l] C. Nicolaou,[j] A. Orlando,[x] D. Palioselitis,[am] K. Papageorgiou,[o] A. Papaikonomou,[d] R. Papaleo,[x] I.A. Papazoglou,[al] G.E. Păvălaş,[ag] H.Z. Peek,[am] J. Perkin,[ap] P. Piattelli,[x] V. Popa,[ag] T. Pradier,[af] E. Presani,[am] I.G. Priede,[a] A. Psallidas,[ao] C. Rabouille,[g] C. Racca,[m] A. Radu,[ag] N. Randazzo,[u] P.A. Rapidis,[al] P. Razis,[j] D. Real,[p] C. Reed,[am] S. Reito,[u] L.K. Resvanis,[d,ao] G. Riccobene,[x] R. Richter,[l] K. Roensch,[l] J. Rolin,[q] J. Rose,[aj] J. Roux,[i] A. Rovelli,[x] A. Russo,[aa] G.V. Russo,[v] F. Salesa,[p] D. Samtleben,[am] P. Sapienza,[x] J.-W. Schmelling,[am] J. Schmid,[l] J. Schnabel,[l] K. Schroeder,[h] J.-P. Schuller,[f] F. Schussler,[f] D. Sciliberto,[u] M. Sedita,[x] T. Seitz,[l] R. Shanidze,[l] F. Simeone,[ad] I. Siotis,[al] V. Sipala,[t] C. Sollima,[ab] S. Sparnocchia,[h] A. Spies,[l] M. Spurio,[s] T. Staller,[ah] S. Stavrakakis,[n] G. Stavropoulos,[ao] J. Steijger,[am] Th. Stolarczyk,[f] D. Stransky,[l] M. Taiuti,[w] A. Taylor,[k] L. Thompson,[ap] P. Timmer,[am] D. Tonoiu,[ag] S. Toscano,[p] C. Touramanis,[ak] L. Trasatti,[y] P. Traverso,[h] A. Trovato,[x] A. Tsirigotis,[o] S. Tzamarias,[o] E. Tzamariudaki,[al] F. Urbano,[p] B. Vallage,[f] V. Van Elewyck,[c] G. Vannoni,[f] M. Vecchi,[i] P. Vernin,[f] S. Viola,[x] D. Vivolo,[aa] S. Wagner,[l] P. Werneke,[am] R.J. White,[aj] G. Wijnker,[am] J. Wilms,[l] E. de Wolf,[b,am] H. Yepes,[p] V. Zhukov,[ao] E. Zonca,[f] J.D. Zornoza[p] and J. Zúñiga[p]

2013 JINST 8 T03006

[a] *University of Aberdeen, Aberdeen, United Kingdom*
[b] *University of Amsterdam, Amsterdam, the Netherlands*
[c] *APC – AstroParticule et Cosmologie – UMR 7164 (CNRS, Université Paris 7, CEA, Observatoire de Paris), Paris, France*
[d] *University of Athens, Athens, Greece*
[e] *University of Barcelona, Barcelona, Spain*
[f] *CEA, IRFU, Centre de Saclay, 91191 Gif-sur-Yvette, France*
[g] *CEA-CNRS-UVSQ, LSCE/IPSL, 91198 Gif-sur-Yvette, France*
[h] *CNR-ISMAR, La Spezia, Trieste, Genova, Italy*
[i] *CPPM, Aix-Marseille Université, CNRS/IN2P3, Marseille, France*
[j] *University of Cyprus, Cyprus*
[k] *Dublin Institute for Advanced Studies (DIAS), Dublin, Ireland*
[l] *Erlangen Centre for Astroparticle Physics (ECAP), University of Erlangen–Nuremberg, Germany*
[m] *Groupe de Recherche en Physique des Hautes Energies (GRPHE)/EA3438/Université de Haute Alsace, Colmar, France*
[n] *Hellenic Centre for Marine Research (HCMR), Greece*
[o] *Hellenic Open University, Patras, Greece*
[p] *IFIC – Instituto de Física Corpuscular, CSIC and Universitat de València, València, Spain*
[q] *IFREMER, France*
[r] *INFN Sezione di Bari and University of Bari, Bari, Italy*
[s] *INFN Sezione di Bologna and University of Bologna, Bologna, Italy*
[t] *INFN Sezione di Cagliari and University of Sassari, Sassari, Italy*
[u] *INFN Sezione di Catania, Catania, Italy*
[v] *INFN Sezione di Catania and University of Catania, Catania, Italy*
[w] *INFN Sezione di Genova and University of Genova, Genova, Italy*
[x] *INFN Laboratori Nazionali del Sud, Catania, Italy*
[y] *INFN Laboratori Nazionali di Frascati, Frascati, Italy*
[z] *INFN Sezione di Napoli, Napoli, Italy*
[aa] *INFN Sezione di Napoli and University of Napoli, Napoli, Italy*
[ab] *INFN Sezione di Pisa and University of Pisa, Pisa, Italy*
[ac] *INFN Sezione di Roma, Roma, Italy*
[ad] *INFN Sezione di Roma and University of Roma 1 "La Sapienza", Roma, Italy*
[ae] *Istituto Nazionale di Geofisica e Vulcanologia (INGV), Italy*
[af] *University of Strasbourg and Institut Pluridisciplinaire Hubert Curien/IN2P3/CNRS, Strasbourg, France*
[ag] *Institute of Space Science, Măgurele-Bucharest, Romania*
[ah] *University of Kiel, Kiel, Germany*
[ai] *KVI, University of Groningen, Groningen, the Netherlands*
[aj] *University of Leeds, Leeds, United Kingdom*
[ak] *University of Liverpool, Liverpool, United Kingdom*
[al] *National Center of Scientific Research "Demokritos", Athens, Greece*
[am] *Nikhef, Amsterdam, the Netherlands*
[an] *Koninklijk Nederlands Instituut voor Onderzoek der Zee (NIOZ), Texel, the Netherlands*
[ao] *NOA/NESTOR, Pylos, Greece*
[ap] *University of Sheffield, United Kingdom*
[aq] *Tecnomare, Venice, Italy*
[ar] *University of Utrecht, Utrecht, the Netherlands*
[as] *Institut d'Investigació per a la Gestió integrada de les Zones Costaneres, Universitat Politècnica València, Gandia, Spain*

2013 JINST 8 T03006

[1] *Also at Université Paris-Sud, 91405 Orsay Cedex, France.*
[2] *Now at Universität Würzburg, Germany.*
[3] *On leave of absence at Humboldt University, Berlin, Germany.*
[4] *Now at Dept. of Physics and Wisconsin IceCube Particle Astrophysics Center, University of Wisconsin, Madison, WI 53706, U.S.A.*
[5] *Also at Moscow State University, Skobeltsyn Institute of Nuclear Physics, Moscow, Russia.*
[6] *Now at Bogolyubov Institute for Theoretical Physics, Ukraine.*
[7] *Now at Laboratoire d'Annecy-le-Vieux de physique des particules (LAPP), France.*
[8] *Now at Institut for Cosmic Ray Research, University of Tokyo, Japan.*
[9] *Now at Université Paris VI, Laboratoire de Physique Nucléaire et de Hautes Energies (LPNHE), France.*

2013 JINST 8 T03006